Physica B 677 (2024) 415711

Contents lists available at ScienceDirect

Physica B: Condensed Matter

journal homepage: www.elsevier.com/locate/physb

Significantly enhanced thermoelectric performance of interstitial N-doped graphene: A density functional theory study

Dwi Nugraheni Rositawati [a,b], Eri Widianto [b,c], Arif Lukmantoro [b], Moh. Adhib Ulil Absor [b], Sholihun [b], Kuwat Triyana [b], Iman Santoso [b,*]

[a] Department of Physics Education, Faculty of Teacher Training and Education, Sanata Dharma University, Jl. Affandi Mrican Tromol Pos 29, Yogyakarta, 55002, Indonesia
[b] Department of Physics, Faculty of Mathematics and Natural Sciences, Universitas Gadjah Mada, Sekip Utara PO Box BLS 21, Yogyakarta, 55281, Indonesia
[c] Department of Mechanical Engineering, Faculty of Engineering, Universitas Singaperbangsa Karawang, Telukjambe Timur, Karawang, 41361, Indonesia

ARTICLE INFO

Keywords:
Graphene
N-doped
Electronic properties
Thermoelectric

ABSTRACT

The thermoelectric characteristics of interstitial nitrogen (N)-doped graphene have been studied using the first principles calculations combined with the semi-classical Boltzmann theory. We found that the Seebeck coefficient of N-doped graphene is 3 and 5.5 times higher compared to pristine graphene, along with *ZT* values. At room temperature, for pristine graphene, the *ZT* value stands at 0.81, whereas it rises to 0.98 and 1.00 for N-doped graphene with 6.25 % and 50 % nitrogen doping, respectively. The increase in the Seebeck coefficient of N-doped graphene is due to the increase in the effective mass band as the chemical potential rises above the conduction band minimum. We observed that N-doped graphene exhibits the highest *ZT* value in the positive energy range, indicating a p-type character. Our findings suggest that *N*-doped graphene has promising potential for thermoelectric applications and provides insights into the underlying physics governing the thermoelectric properties of doped graphene materials.

1. Introduction

The potential of thermoelectric materials to convert waste heat into valuable electrical energy has garnered significant interest due to their ability to contribute to energy sustainability and mitigate greenhouse gas emissions. Advancements in materials science and device structures have recently resulted in significant strides in enhancing the performance index (referred to as the figure of merit or *ZT*) of thermoelectric devices. The performance of thermoelectric materials is determined by the dimensionless figure of merit *ZT* as follows:

$$ZT = \frac{S^2\sigma}{\kappa}T = \frac{S^2\sigma}{\kappa_{el} + \kappa_{lat}}T \quad (1)$$

where S is the Seebeck coefficient, σ is the electric conductivity, T is the absolute temperature, and κ is the thermal conductivity [1–8]. As a relatively independent coefficient among the fundamental physical quantities of thermoelectric materials, lattice thermal conductivity (κ_{lat}) is essential for improving thermoelectric performance [9]. The thermal conductivity κ is obtained from the contribution of electrons and phonons, $\kappa = \kappa_e + \kappa_{ph}$. From equation (1), it can be seen that the material that can be used for thermoelectric applications is a material that has a high *ZT* value, which can be obtained from materials that have large S, high σ, and low κ, simultaneously. The rapid development of the thermoelectric device accelerates the possible commercial applications, which need excellent thermal stability and mechanical properties [9,10].

Thermoelectric devices commonly utilize inorganic substances such as Tellurium (Te), Lead (Pb), and Bismuth (Bi). However, these materials have several drawbacks, including toxicity and the need for costly processes conducted in high-temperature and vacuum environments [11,12]. However, there has been significant research on organic compounds, such as polypyrrole [13,14], poly(3,4-ethylenedioxythiophene):poly(styrenesulfonate) (PEDOT:PSS) [15], and polyaniline (PANI) [16,17]. A low-temperature solution technique can be used to make inexpensive thermoelectric devices made of organic materials. These materials are ideal for usage in thermoelectric power generators used into wearable smart devices to their outstanding mechanical flexibility. However, in general, these materials have low

* Corresponding author.
E-mail address: iman.santoso@ugm.ac.id (I. Santoso).

https://doi.org/10.1016/j.physb.2024.415711
Received 22 July 2023; Received in revised form 19 January 2024; Accepted 21 January 2024
Available online 22 January 2024

electrical conductivity. Many methods have been used to overcome this problem, including doping and mixing with inorganic materials [15,18–20]. However, the increase in conductivity due to doping causes the value of the Seebeck coefficient to decrease [21]. In addition, organic thermoelectric materials have unstable atmospheric conditions.

Two-dimensional (2D) materials are novel materials that can be used as thermoelectric devices [19,22–26]. They exhibit excellent mechanical properties, good air stability, and strong electrical conductivity. Among the currently available 2D materials, graphene, and MXene families have attracted extensive attention due to their properties, including high mobility of charge carriers [27–29], transfer capability to other substrates, and easy-to-modulate electrical properties [18,19,30]. Graphene, as a 2D material having unique thermal, mechanical, and electronic properties, has been proposed as a potential thermoelectric material [24–26,31,32].

However, graphene has a zero band gap and very high thermal conductivity, causing attention to graphene as a thermoelectric material to tend to diminish [33–36], especially due to pristine graphene has a low thermoelectric figure of merit (*ZT*), which further limits its application as a thermoelectric material. In recent years, the electrical and thermoelectric characteristics of graphene have attracted great interest [37,38]. Various efforts are used to improve the thermoelectric performance of graphene materials, namely by increasing electrical conductivity and, at the same time, lowering its thermal conductivity. Initially, the *ZT* value of pristine graphene at room temperature [39] was found to be 0.55×10^{-3}, which is far below the commercially desirable $ZT \approx 4$. *ZT* increases three times higher than pristine graphene by treating oxygen plasma treated graphene with a sufficiently high defect density [39], implying that introducing a controlled number of defects into graphene is an effective way to improve thermoelectric performance.

Recent studies have shown that significantly doping graphene with heteroatoms can improve thermoelectric performance [40,41]. The first theoretical study on thermoelectric devices using nanoscale thin-coated graphene is predicted to have a maximum *ZT* value of ~3 at ambient temperature with proper chemical functionalization (hydrogen and pentane) [25]. Nano-ribbons of single-layer graphene can be used to increase *ZT* enhancements of up to 2 by altering the nanopores to the proper dimension and adding them to the nanoribbon structure [42]. Although encouraging, these predictions have not come to pass since it is challenging to create a large-area monolayer graphene sheet thermoelectric device with more heat absorption than nanoscale devices [23,43]. A large-area thermoelectric device that makes p and n junctions using chemical doping and reduced graphene oxide (rGO) [44]. Although this large-area device's performance was higher than that of a nanoscale device, it was still lower than the single-layer graphene value predicted by theory. For graphene-based thermoelectric devices, several alternative conductivity-enhancement techniques have been reported, including spray-coating with Au nanoparticles to improve doping and employing O_2 plasma to create porous graphene or Au/graphene/hBN stacked structures [39,45,46].

In general, chemical doping using nitrogen (N) or boron (B) is widely regarded as an excellent way to modify the characteristics of graphene-based materials [47,48]. Nitrogen doping plays a crucial role in shaping the characteristics of carbon compounds due to its similar atomic size and the presence of five valence electrons, enabling robust valence bonds with carbon atoms. Theoretical investigations have revealed that nitrogen doping leads to an amplified positive charge on a carbon atom near nitrogen atoms [49] and a favorable shift in the Fermi energy at the apex of the Brillouin zone of graphene [50]. Peng et al. were the first to disclose the production of N-doped graphene, which they used as electrocatalysts in an oxygen reduction process [49]. This has attracted much interest, making N-doped graphene even more popular. Various techniques have been utilized to fabricate N-doped graphene, such as wet chemical synthesis [51], chemical vapor deposition (CVD) [52–57], a solvothermal method [58–60], thermal annealing [47,61,62], a hydrothermal process [63], pyrolysis [64,65], plasma treatment [66,67], arc-discharge [66,68], N_2H_4 treatment [69–71]. As a result, it is critical to explore how nitrogen doping affects the structure of graphene and how chemical characteristics might be correspondingly altered. However, to date, only a limited number of studies have been conducted on the design and thermoelectric features of N-doped graphene.

In this work, we investigate the electronic and thermoelectric properties of N-doped graphene using first-principles calculations. Our study aims to provide a fundamental understanding of the underlying physics governing the thermoelectric performance of N-doped graphene, which can guide the design and development of new and efficient thermoelectric materials. Specifically, we focus on the interstitial doping effect of N-doped graphene (2 and 16 N dopant atom), which has exhibited a higher *ZT* in comparison to pristine graphene. The introduction of N atoms leads to the opening of the band gap at the *K*-point of the Brillouin zone and the formation of localized states near the Fermi level, which shifts the band gap above the Fermi level, leading to an increase of charge carrier, which in turn enhanced the Seebeck coefficient. Furthermore, N-doped graphene can exhibit low thermal conductivity due to phonon scattering by the N dopants and the modification of the graphene lattice structure [72,73]. Our results show that N-doped graphene exhibits a high thermoelectric performance, which suggests its potential for thermoelectric applications.

2. Computational details

2.1. Geometry and electronic structure

The 4×4 graphene supercell (consisting of 32C atoms) and nitrogen atoms as the interstitial doping atom are used to represent the N-doped graphene supercell systems. In the z-axis direction, there is a vacuum parameter of 25 Å to prevent interlayer interactions. The pristine graphene supercell is optimized by fully relaxing atoms till the Hellmann-Feynman force component acting on each atom is less than 10^{-5} Ha/Bohr. Specifically, on the x- and y-axes, doping positions are fixed, and on the z-axis, they are relaxed [74–76]. The interstitial doping effect is studied at dopant concentrations of 6.25 % (two nitrogen atoms in 32 carbon atoms) and 50 % (sixteen nitrogen atoms in 32 carbon atoms), which have the lowest total energy.

The geometry optimization and electronic structure of N-doped graphene are calculated using the DFT [77–80], which is carried out in the OpenMX code [81]. It is based on pseudo-atomic localized basis functions [82,83] and norm-conserving pseudopotential [84]. The basis functions' precision, such as the pseudopotentials (VPS), the delta gauge approach utilize carefully benchmarked [85], after which a linear combination of several pseudoatomic orbitals (PAO) expand the basis functions using a confinement scheme [82,83]. The pseudo-atomic orbital basis functions are C6.0-s3p2d2 and N6.0-s3p2d2. The generalized gradient approximation (GGA) of Perdew-Burke-Ernzerhof (PBE) [86] analyzes the interplay between electronic exchange and correlation. The 300 Ry cut-off energy and energy convergence threshold of 1×10^{-9} Hartree are applied in all calculations. An $8 \times 8 \times 1$ *K*-grid with the gamma (Γ) as its center is used to sample the first Brillouin Zone. The N-doped graphene's density of states (DOS) and partial density of states (PDOS) are calculated using the $12 \times 12 \times 1$ *K*-grid.

2.2. Thermoelectric properties

The thermoelectric properties are calculated by determining electron transport coefficients based on the semi-classical Boltzmann theory (where the carriers' relaxation time is τ) from the wave number dependence of the energy eigenvalues in the Kohn-Sham equation, OpenMX is interfaced with BoltzTraP [82,87,88]. BoltzTraP software is used as a post-processing tool to calculate thermoelectric properties through physical quantities as well as relative electrical conductivity $\sigma\tau^{-1}$, the Seebeck coefficient *S*, and electronic thermal conductivity κ_e

which depends on the chemical potential μ, which can be determined by using the following equations [88]:

$$K_n = \int \sigma(\varepsilon, T)(\varepsilon - \mu)^n \left(-\frac{\partial f_{FD}}{\partial \varepsilon} \right) \partial \varepsilon, \tag{2}$$

$$\sigma(T) = K_0, S(T) = -\frac{1}{|e|T}\frac{K_1}{K_0}, \kappa_e(T) = \frac{1}{|e|^2 T}\left(K_2 - \frac{K_1^2}{K_0}\right) \tag{3}$$

where K_n is the transport coefficient, $\sigma(\varepsilon, T)$ is the conductivity spectrum at ε and T, ε is the energy, f_{FD} is the Fermi–Dirac distribution function, μ is the chemical potential, e is the elementary electric charge, and T is the absolute temperature.

3. Result and discussion

3.1. Geometrical structures

The optimized pristine graphene and N-doped graphene supercell systems are illustrated in the left panel of Fig. 1(a–c). The calculated lattice parameter for the 4 × 4 pristine graphene supercell structure is 9.89 Å. This is very much in agreement with the earlier results [74,89]. The interstitial doping effect is studied at dopant concentrations of 6.25 % and 50 % in 32C atoms, which have the lowest total energy. Table 1 shows the total energy for 6.25 % N is −5630.053 eV and −9438.098 eV for 50 % N. The bridge site is the most stable site for N doping [75]. As the doping concentration increases, the total energy decreases. The distance between the two nearest carbon atoms (d_{CC}) was found to have the same value when dopant atoms were added to graphene. The increase in doping concentration causes a decrease in the height position of N doping from C atoms (h), particularly the distance of the N doping from its closest carbon atoms (d_{DC}).

Table 1
The structural properties of N doping at the bridge sites (B) listed are the distance between the two nearest carbon atoms (d_{CC}); the height position of N doping from C atoms (h); the distance of the N doping from its closest carbon atoms (d_{DC}); and the total energy (E_{tot}).

Number of dopant atom	Doping concentration (%)	d_{CC} (Å)	h (Å)	d_{DC} (Å)	E_{tot} (eV)
2	6.25	1.43	1.37	1.54	−5630.053
16	50	1.43	1.30	1.48	−9438.098

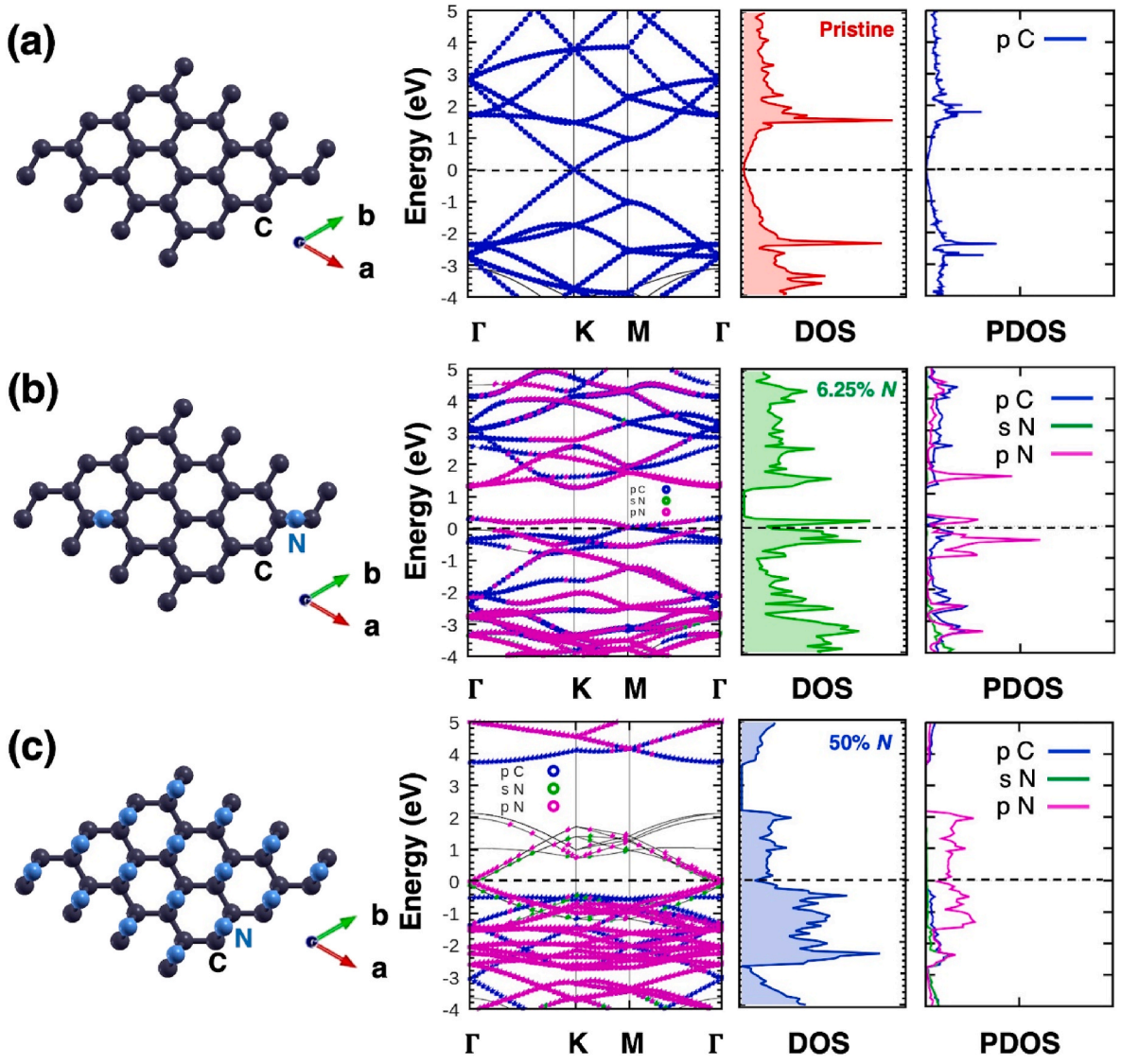

Fig. 1. Structure, projected band structure, the density of states (DOS), and PDOS for **(a)** pristine graphene, **(b)** 6.25 % *N*-doped graphene, and **(c)** 50 % *N*-doped graphene. The black and blue atoms are carbon and nitrogen atoms, respectively.

3.2. Electronic properties

Fig. 1 shows the projected band structures, DOS, and PDOS of pristine and N-doped graphene supercells. Both samples of N-doped graphene supercell exhibit the energy band gaps of 0.7 eV and 1.4 eV for 6.25 % N-doped and 50 % N-doped, respectively, which are shifted away above the Fermi level. For 6.25 % N-doped, the band gap is formed by both the p-orbital of a carbon atom and the p-orbital of an N atom, while the band gap for 50 % N-doped is formed by the p-orbital of a carbon atom (minimum of conduction band) and p-orbital of N atom (maximum of valence band) which is in accordance with DOS calculations (Fig. 1 (c)). The transfer of charge from graphene to the N atom causes a shift in the Fermi level in the N-doped graphene system, whose value increases with increasing doping concentration. We observe that the Fermi level is shifting away about 0.7 eV and 1.9 eV for 6.25 % and 50 % N-doped graphene, respectively, indicating that N-doped graphene is electron-deficient. This implies that graphene with interstitial N doping has the p-type character of charge carrier, which contrasts with substitutional N-doped graphene [90].

The DOS and PDOS data show localized states at energy levels of ~ -0.3 eV and 1.6 eV for 6.25 % N-doped graphene (Fig. 1 (b)). From our calculation, both localized states are due to the 2p orbital of N. As for 50 % N-doped graphene, the localized state at the Fermi energy disappears. The 2p orbital of the N atom determines the state at the Fermi level for this concentration, which leads to poorer transport properties. The difference in work function between graphene and the atomic dopant as well as the electron affinity of the atomic dopant causes a shift in the Fermi level and charge transfer [74]. The charge density difference of N-doped graphene is plotted using VESTA software as follows (Fig. 2).

The amount of charge transfer between two systems can be determined with *ECT* following [91]:

$$ECT = (\Delta N_{max})_A - (\Delta N_{max})_B \tag{4}$$

where ΔN_{max} is the maximum electronic charge ($\Delta N_{max} = -\mu/\eta$), μ is chemical potential, and η is the chemical hardness of the system. According to equation (4), the *ECT* value of 6.25 % *N*-doped graphene is 0.082*e*. This means that each nitrogen atom receives 0.041*e* from graphene. Meanwhile, the *ECT* value of 50 % *N*-doped graphene is 0.72*e,* where each nitrogen atom receives 0.045*e* from graphene. Thus, graphene acts as an electron donor on 6.25 % and 50 % N-doped graphene.

3.3. Thermoelectric properties

In this section, we study the thermoelectric properties of the N-doped graphene supercell systems, how the chemical potential affects transport properties that include the Seebeck coefficient (*S*), a figure of merits (*ZT*), electrical conductivity (σ/τ), thermal conductivity (κ_e/τ), and also a number of charge carriers per unit cell (*N*) of N-doped graphene at 300 *K*. The transport properties are calculated from −2 eV to 4 eV. It is presumptively ignored how phonon thermal conductivity contributes. Fig. 3 (a, e, i) and Fig. 4 (a) show the calculated temperature-dependent electrical conductivity ($\sigma\tau^{-1}$) while Fig. 3 (b, f, j) and Fig. 4 (b) show the thermal conductivity (κ_e/τ) versus chemical potential μ for pristine, 6.25 % N-doped graphene and 50 % N-doped graphene, respectively. Near the Fermi level, electrical conductivity and thermal conductivity exhibit roughly symmetric behavior [92] for pristine graphene, which is due to the symmetric DOS around the Fermi level. For 6.25 % N-doped graphene, the DOS around the Fermi level becomes less symmetrical, and it shifts according to the shifting of the band gap observed in DOS. Doping graphene with 50 % nitrogen atom results in more asymmetrical electrical conductivity, shifting further away from the Fermi level, which is in accordance with DOS, indicating the p-type character of charge carrier in N-doped graphene. The electrical conductivity for pristine, 6.25 %, and 50 % N-doped graphene seem not affected by temperature changes except at the band gap, where it starts to be filled by the charge carrier. An increase in nitrogen concentration causes an increase in electrical conductivity around the Fermi level; at the same time, it rises as the temperature increases (see Fig. 4 (a)), representing better transport properties.

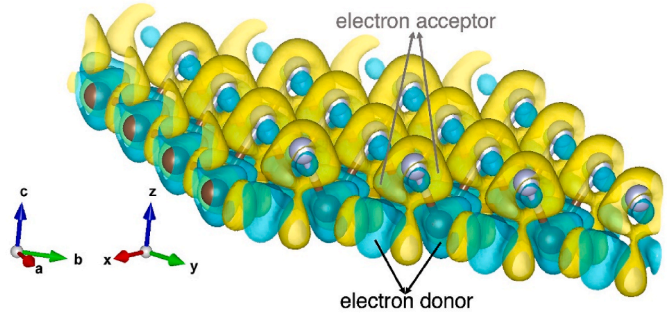

Fig. 2. Charge density difference of *N*-doped graphene.

In terms of thermal conductivity, it exhibits a more pronounced temperature dependence, increasing as the temperature rises for pristine graphene, as well as for graphene doped with 6.25 % and 50 % nitrogen. Notably, the thermal conductivity follows the same behavior as electrical conductivity (Fig. 4(a) and (b)). The system under study adheres to the Wiedemann–Franz Law Law ($\kappa_e = L\sigma T$; where *L* is the Lorentz number), which makes the optimization of thermoelectric properties a complex task [88]. Seebeck coefficient is a parameter to identify majority and minority charge carriers. We have plotted the temperature dependence of the Seebeck coefficient (*S*) of pristine graphene, 6.25 % N-doped graphene, and 50 % N-doped graphene versus chemical potential μ, as shown in Fig. 3 (c, g, k). The maximum value of *S* at $T = 300\ K$ for pristine graphene is 464 $\mu V/K$, and it increases to 1488 $\mu V/K$ and 2539 $\mu V/K$ for 6.25 % and 50 % N-doped graphene, respectively. The characteristic Seebeck coefficient can be understood from DOS. By considering the charge carriers in the region around the Fermi level that contribute to the conduction process, the Fermi level shifts following the addition of doping concentration, and DOS becomes asymmetric around E_F, leading to the asymmetrical *S* around E_F. The increase in the Seebeck coefficient of N-doped graphene is also due to the increase in the effective mass band as the chemical potential rises above the conduction band minimum, as shown in Fig. 1 (projected band structure and DOS). Fig. 3 (c, g, k) also shows that the maximum value of the Seebeck coefficient is at a positive chemical potential value [93] indicating the p-type behavior of N-doped graphene. A material with a large band gap typically has a large Seebeck coefficient [42], where the relationship between *S* and E_g can be understood by $S \approx -(k_B/e)(E_g/2k_BT+2)$ [2, 94]. Note that in our case, the band gap is shifted away from the Fermi level. This is why we found that the largest optimum *S* is owned by 50 % N-doped graphene since $E_{g_{50\%\ N}} > E_{g_{6.25\%\ N}} > E_{g_{pristine}}$. Fig. 4 (c) shows that the increase in temperature causes the maximum value of *S* for pristine graphene, 6.25 % N-doped graphene, and 50 % N-doped graphene to decrease due to the addition of hole concentration (see Fig. 5).

We evaluated the performance of thermoelectric materials by using Equation (1) to calculate a dimensionless figure of merit (*ZT*). In Fig. 3 (d, h, l) and Fig. 4 (d), we observed that N-doped graphene exhibits the highest *ZT* value in the positive energy range, indicating a p-type character. This enhanced *ZT* value is attributed to the significantly increased electrical conductivity resulting from the larger effective mass band in DOS. Adding a dopant can adjust the carrier concentration and increase the degeneration of the band to increase the charge carrier's effective mass [95–98]. Furthermore, Fig. 3 (d, h, l) demonstrates that the *ZT* value rises with increasing dopant concentration [98], and the *ZT* width becomes wider as the doping level increases, which is likely due to the rise of band gap.

The characteristic of *ZT* can be understood from DOS. Considering the charge carriers in the region around the Fermi level that contribute

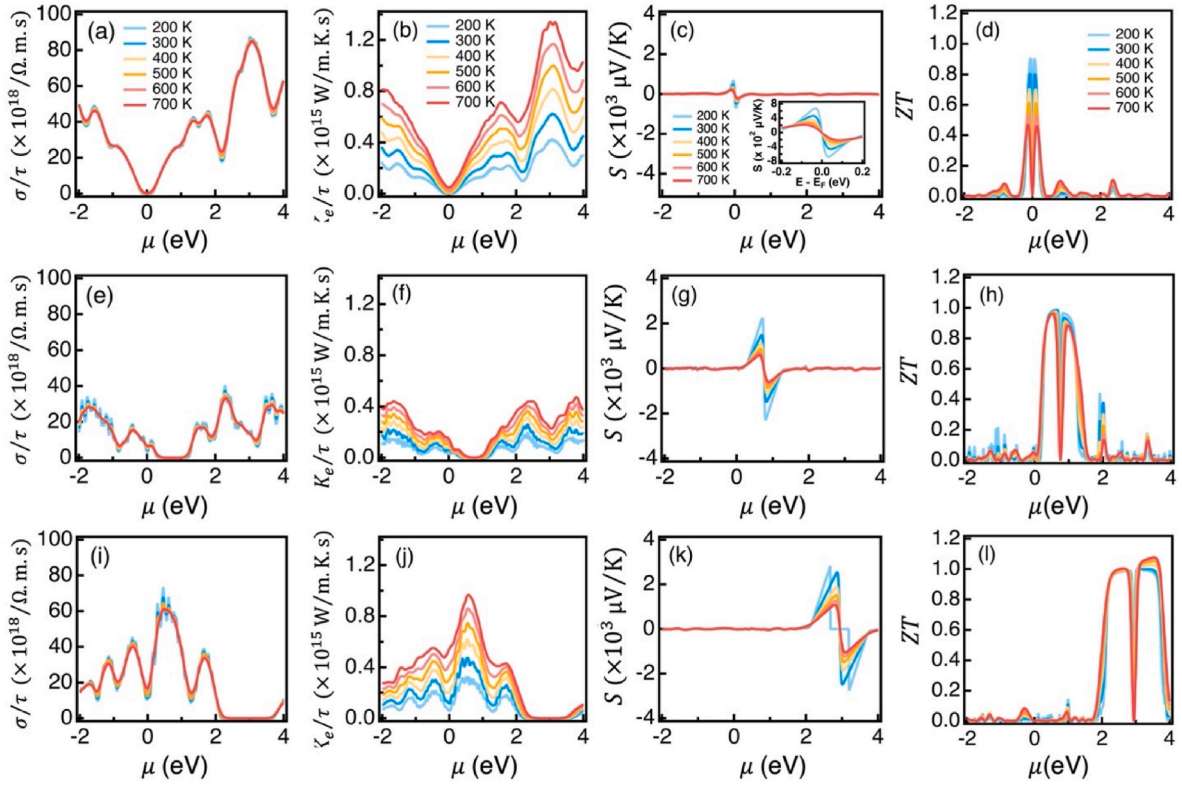

Fig. 3. (**Upper panel)** Calculated temperature dependence of **(a)** electrical conductivity, **(b)** thermal conductivity, **(c)** Seebeck coefficient, **(d)** figure of merit of pristine graphene. (**Middle panel)** Calculated temperature dependence of **(e)** electrical conductivity, **(f)** thermal conductivity, **(g)** Seebeck coefficient, **(h)** figure of merit of 6.25 % N-doped graphene. (**Lower panel)** Calculated temperature dependence of **(i)** electrical conductivity, **(j)** thermal conductivity, **(k)** Seebeck coefficient, **(l)** figure of merit of 50 % N-doped graphene.

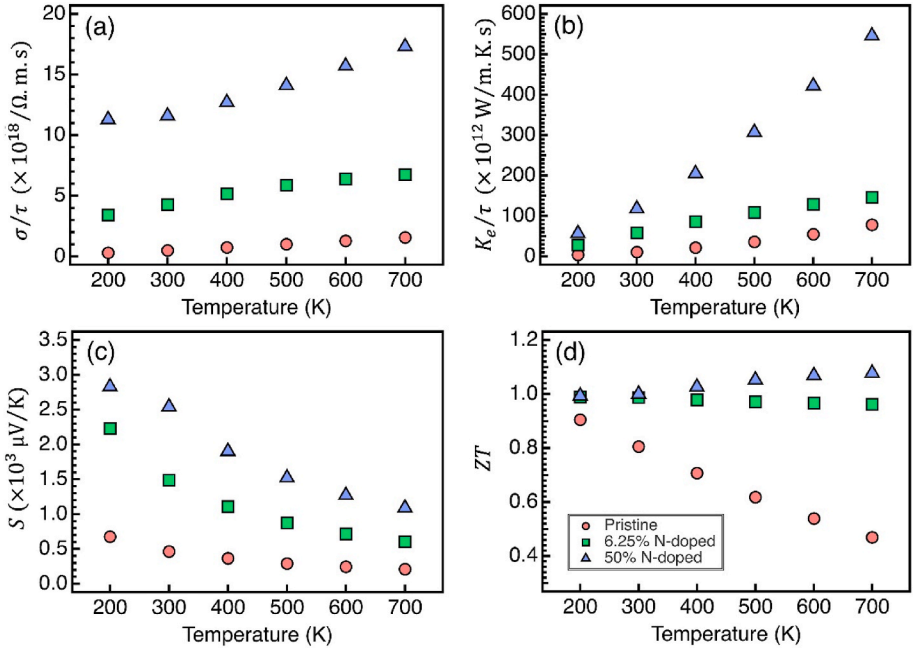

Fig. 4. Calculated temperature dependence of maximum **(a)** electrical conductivity, **(b)** thermal conductivity, **(c)** Seebeck coefficient, **(d)** figure of merit as a function of temperature.

to the conduction process, the Fermi level shifts following the addition of doping concentration, and DOS becomes asymmetric around E_F. It causes characteristic ZT also to be asymmetric around E_F. Fig. 4 (d) shows an increase in temperature gives the same trend between pristine and 6.25 % N-doped graphene; namely, an increase in temperature causes a decrease in the value of ZT, but it does not apply to 50 % N-doped graphene. The ZT feature for 50 % N-doped graphene behaves differently due to the higher rate of temperature dependence of thermal

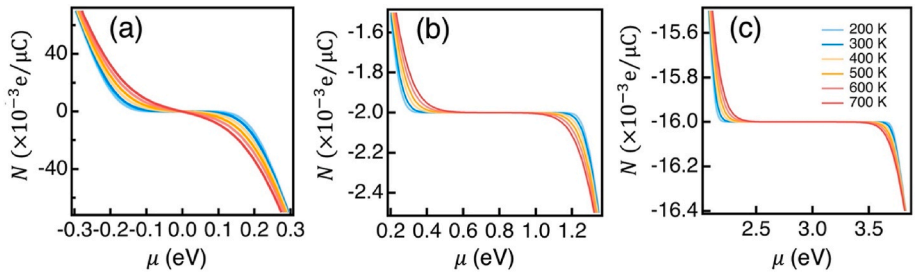

Fig. 5. Calculated temperature dependence of the number of charge carriers per unit cell *N* for **(a)** pristine graphene, **(b)** 6.25 % N-doped graphene, and **(c)** 50 % N-doped graphene.

conductivity and Seebeck coefficient (Fig. 3 (j and k)) as compared to pristine and 6.25 % N-doped graphene.

Moreover, the *ZT* value is influenced by temperature, meaning that when combined with κ_e/τ and *S*, their product will lead to an enhanced *ZT* as the temperature rises. At room temperature, for pristine graphene, the *ZT* value is 0.81, which improves to 0.98 and 1.00 for N-doping of 6.25 % and 50 %, respectively. Hence, N-doped graphene emerges as a promising thermoelectric material, achieving a *ZT* value of 1 [92]. Note that for 50 % N-doped graphene, the highest *ZT* energy state is located at a significantly deep energy level, making it would be exceptionally challenging to access experimentally. However, for other systems such as Ge-intercalated graphene [99] and K–Ca intercalated graphene [100], the shift of chemical potential as large as 3 eV has been realized. To date, the Fermi level shift for nitrogen doped graphene is approaching 1 eV [101–104]. A comparison of graphene and 2D materials-based thermoelectric properties of our results and other thermoelectric devices is presented in Table 2.

While 2D-based materials, such as graphene, are currently widely studied and demonstrate particularly competitive performance compared to their conventional bulk semiconductor counterparts, there are significant challenges to overcome before practical applications can be realized. One of the essential components in 2D devices that influences the transfer of charge carriers from metal to the 2D pathway is the contact between semiconductors and metal electrodes [116,117]. The interfacial injection of charge in 2D materials has a crucial effect on several device figure of merit, including contact resistance and the current on/off ratio. Consequently, it is critical to develop effective contact engineering methodologies for establishing ohmic contacts in 2D devices. Although further studies on thermoelectric performance are necessary, these results confirm the underlying physics governing the thermoelectric properties of N-doped graphene and suggest its potential for thermoelectric applications.

4. Conclusion

In summary, our first-principles study demonstrates that N-doped graphene has promising thermoelectric properties, especially in the interstitial doping effect. We found that the Seebeck coefficient of N-doped graphene is 3 and 5.5 times higher compared to pristine graphene, along with *ZT* values. For pristine graphene, the *ZT* value stands at 0.81, whereas it rises to 0.98 and 1.00 for N-doped graphene with 6.25 % and 50 % nitrogen doping, respectively. The increase in the Seebeck coefficient of N-doped graphene is due to an increase in the effective mass band as the chemical potential rises above the conduction band minimum. We observed that N-doped graphene exhibits the highest *ZT* value in the positive energy range, indicating a *p*-type character. This enhanced *ZT* value is attributed to the significantly increased electrical conductivity resulting from the larger effective mass band in DOS. This enhanced *ZT* value of N-doped graphene is attributed to the significantly increased electrical conductivity resulting from the larger effective mass band in DOS. The formation of localized states near the Fermi level due to the introduction of N atoms increases the density of states, which enhances the Seebeck coefficient. Our findings provide insights into the underlying physics governing the thermoelectric properties of N-doped graphene and suggest its potential for thermoelectric applications. Further studies can be conducted to explore the feasibility of N-doped graphene as a practical thermoelectric material and to optimize its thermoelectric performance for various applications.

Table 2
Thermoelectric properties of graphene and 2D materials devices.

Material	*S* ($\mu V/K$)	*PF* ($\mu W/mK^2$)	*ZT*	References
PAA-doped Graphene	350	14000	–	[19]
Graphene-nanoribbon	30	1.8	–	[45]
PEI-doped rGO	16.9	–	–	[46]
Au/h-BN/Graphene	215	–	–	[105]
Graphene sheet	40–60	1000–5000	–	[106]
PANi/Graphene	15	19	–	[107]
n-Cr_2TiC_2	930	–	0.4	[108]
p-$Ti_2MoC_2F_2$	150	–	3.1	[109]
$Ti_3C_2T_x$/BST	192	–	0.65	[110]
Graphene/MoS_2	–	–	2.8	[111]
Graphene/Phosphorous	118	–	0.13	[112]
WSe_2/$MoSe_2$	375	–	3.4	[113]
MgO(100)	298	–	1.5	[114]
MoSSe	157	240	0.013	[115]
C– MoSSe	238	3410	0.18	[115]
Pristine graphene	464	–	0.81	This work
6.25 % N-doped graphene	1488	–	0.98	This work
50 % N-doped graphene	2539	–	1.00	This work

CRediT authorship contribution statement

Dwi Nugraheni Rositawati: Conceptualization, Data curation, Formal analysis, Writing – original draft, Writing – review & editing. **Eri Widianto:** Validation, Visualization, Writing – review & editing. **Arif Lukmantoro:** Data curation, Methodology, Software. **Moh. Adhib Ulil Absor:** Methodology, Software, Validation. **Sholihun:** Methodology, Software, Validation, Methodology, Software, Validation. **Kuwat Triyana:** Supervision, Validation. **Iman Santoso:** Project administration, Supervision, Validation, Writing – review & editing.

Declaration of competing interest

The authors declare that they have no known competing financial interests or personal relationships that could have appeared to influence the work reported in this paper.

Data availability

Data will be made available on request.

Acknowledgements

We wish to acknowledge Masanobu Miyata and Yung-Ting Lee for

fruitful discussions about the BoltzTraP interface program to determine the thermoelectric properties of material. This work was supported by the Indonesian Ministry of Education and Culture through the BPPDN-2019 (Beasiswa Pendidikan Pascasarjana Dalam Negeri) scholarship program.

References

[1] P. Lubis, N. Amalia, S.A. Wella, S. Sholihun, Thermoelectric properties of monolayer and bilayer buckled XTe (X = Ge, Sn, and Pb), Adv. Nat. Sci. Nanosci. Nanotechnol. 13 (2022), https://doi.org/10.1088/2043-6262/ac7322.

[2] K.-X. Chen, S.-S. Lyu, X.-M. Wang, Y.-X. Fu, Y. Heng, D.-C. Mo, Excellent thermoelectric performance predicted in two-dimensional buckled Antimonene: a first-principles study, J. Phys. Chem. C 121 (2017) 13035–13042, https://doi.org/10.1021/acs.jpcc.7b03129.

[3] D. Singh, R. Ahuja, Enhanced optoelectronic and thermoelectric properties by intrinsic structural defects in monolayer HfS_2, ACS Appl. Energy Mater. 2 (2019) 6891–6903, https://doi.org/10.1021/acsaem.9b01402.

[4] B. Ul Haq, S. AlFaify, T. Alshahrani, R. Ahmed, Q. Mahmood, S.A. Tahir, H. H. Alhashim, A. Laref, Exploring the potential of lead-chalcogenide monolayers for room-temperature thermoelectric applications, Ceram. Int. 47 (2021) 3380–3388, https://doi.org/10.1016/j.ceramint.2020.09.183.

[5] D.D. Fan, H.J. Liu, L. Cheng, P.H. Jiang, J. Shi, X.F. Tang, MoS_2 nanoribbons as promising thermoelectric materials, Appl. Phys. Lett. 105 (2014), https://doi.org/10.1063/1.4897349.

[6] D. Zhang, S. Hu, Y. Sun, X. Liu, H. Wang, H. Wang, Y. Chen, Y. Ni, XTe (X = Ge, Sn, Pb) monolayers: promising thermoelectric materials with ultralow lattice thermal conductivity and high-power factor, ES Energy & Environment (2020), https://doi.org/10.30919/esee8c934.

[7] A. Ghadri, A. Boochani, A. Hojabri, F. Hajakbari, Electronic, optical and thermoelectric properties of WSe_2–InN 2D interface: a DFT study, Solid State Commun. 354 (2022) 114889, https://doi.org/10.1016/j.ssc.2022.114889.

[8] N. Hung, A.R.T. Nugraha, T. Yang, Z. Zhang, R. Saito, Thermoelectric performance of monolayer InSe improved by convergence of multivalley bands, J. Appl. Phys. 125 (2019), https://doi.org/10.1063/1.5040752.

[9] C.D. Zhou, B. Liang, W.J. Huang, J.G. Noudem, X.J. Tan, J. Jiang, Phonon engineering significantly reducing thermal conductivity of thermoelectric materials: a review, Rare Met. (2023), https://doi.org/10.1007/s12598-023-02302-3.

[10] X. Bao, S. Hou, Z. Wu, X. Wang, L. Yin, Y. Liu, H. He, S. Duan, B. Wang, J. Mao, F. Cao, Q. Zhang, Mechanical properties of thermoelectric generators, J. Mater. Sci. Technol. 148 (2023) 64–74, https://doi.org/10.1016/j.jmst.2022.10.081.

[11] C.M. Jaworski, J.P. Heremans, Thermoelectric transport properties of the n-type impurity Al in PbTe, Phys. Rev. B 85 (2012) 033204, https://doi.org/10.1103/PhysRevB.85.033204.

[12] R. Basu, S. Bhattacharya, R. Bhatt, M. Roy, S. Ahmad, A. Singh, M. Navaneethan, Y. Hayakawa, D.K. Aswal, S.K. Gupta, Improved thermoelectric performance of hot pressed nanostructured n-type SiGe bulk alloys, J Mater Chem A Mater 2 (2014) 6922, https://doi.org/10.1039/c3ta14259k.

[13] L. Wang, F. Liu, C. Jin, T. Zhang, Q. Yin, Preparation of polypyrrole/graphene nanosheets composites with enhanced thermoelectric properties, RSC Adv. 4 (2014) 46187–46193, https://doi.org/10.1039/C4RA07774A.

[14] L. Liang, G. Chen, C.-Y. Guo, Enhanced thermoelectric performance by self-assembled layered morphology of polypyrrole nanowire/single-walled carbon nanotube composites, Compos. Sci. Technol. 129 (2016) 130–136, https://doi.org/10.1016/j.compscitech.2016.04.023.

[15] E. Jin Bae, Y. Hun Kang, K.-S. Jang, S. Yun Cho, Enhancement of thermoelectric properties of PEDOT:PSS and tellurium-PEDOT:PSS hybrid composites by simple chemical treatment, Sci. Rep. 6 (2016) 18805, https://doi.org/10.1038/srep18805.

[16] Q. Yao, Q. Wang, L. Wang, L. Chen, Abnormally enhanced thermoelectric transport properties of SWNT/PANI hybrid films by the strengthened PANI molecular ordering, Energy Environ. Sci. 7 (2014) 3801–3807, https://doi.org/10.1039/C4EE01905A.

[17] D. Yoo, J.J. Lee, C. Park, H.H. Choi, J.-H. Kim, N-type organic thermoelectric materials based on polyaniline doped with the aprotic ionic liquid 1-ethyl-3-methylimidazolium ethyl sulfate, RSC Adv. 6 (2016) 37130–37135, https://doi.org/10.1039/C6RA02334G.

[18] S. Kim, J. Hwang, Y.J. Kim, H.J. Hwang, M. Son, N. Revannath, M. Ham, K. Cho, B.H. Lee, Threshold voltage modulation of a graphene–ZnO barristor using a polymer doping process, Adv Electron Mater 5 (2019) 1800805, https://doi.org/10.1002/aelm.201800805.

[19] H.J. Hwang, S.-Y. Kim, S.K. Lee, B.H. Lee, Large scale graphene thermoelectric device with high power factor using gradient doping profile, Carbon N Y 201 (2023) 467–472, https://doi.org/10.1016/j.carbon.2022.09.048.

[20] S.Y. He, H.L. Shi, J. Yang, Y.H. Ren, Q.Z. Han, L.J. Gong, Y.H. Zhao, Z.T. Jiang, A comparative investigation into the thermoelectric properties of doped graphene nanoribbons in different doping manners, Diam. Relat. Mater. 135 (2023) 109889, https://doi.org/10.1016/j.diamond.2023.109889.

[21] G.J. Snyder, E.S. Toberer, Complex thermoelectric materials, Nat. Mater. 7 (2008) 105–114, https://doi.org/10.1038/nmat2090.

[22] H. Jang, Y.J. Park, X. Chen, T. Das, M.-S. Kim, J.-H. Ahn, Graphene-based flexible and stretchable electronics, Adv. Mater. 28 (2016) 4184–4202, https://doi.org/10.1002/adma.201504245.

[23] Y. Zhang, H. Han, N. Wang, P. Zhang, Y. Fu, M. Murugesan, M. Edwards, K. Jeppson, S. Volz, J. Liu, Improved heat spreading performance of functionalized graphene in microelectronic device application, Adv. Funct. Mater. 25 (2015) 4430–4435, https://doi.org/10.1002/adfm.201500990.

[24] E. Muchuweni, E.T. Mombeshora, Recent advances in thermoelectric performance by incorporating graphene-based materials for energy harvesting, Renewable Energy Focus 45 (2023) 40–52, https://doi.org/10.1016/j.ref.2023.02.005.

[25] J.Y. Kim, J.C. Grossman, High-efficiency thermoelectrics with functionalized graphene, Nano Lett. 15 (2015) 2830–2835, https://doi.org/10.1021/nl504257q.

[26] T.A. Amollo, G.T. Mola, M.S.K. Kirui, V.O. Nyamori, Graphene for thermoelectric applications: prospects and challenges, Crit. Rev. Solid State Mater. Sci. 43 (2018) 133–157, https://doi.org/10.1080/10408436.2017.1300871.

[27] H. Alavi-Rad, A. Kiani-Sarkaleh, S. Rouhi, A. Ghadimi, Investigation of the electronic and thermoelectric properties of hydrogenated monolayer germanene under biaxial tensile and compressive strains by DFT approach, Physica E Low Dimens Syst Nanostruct 124 (2020) 114339, https://doi.org/10.1016/j.physe.2020.114339.

[28] A. Zarepour, S. Ahmadi, N. Rabiee, A. Zarrabi, S. Iravani, Self-healing MXene- and graphene-based composites: properties and applications, Nano-Micro Lett. 15 (2023) 100, https://doi.org/10.1007/s40820-023-01074-w.

[29] Z. Li, X. Chao, A. Balilonda, W. Chen, Scalable van der Waals graphene films for electro-optical regulation and thermal camouflage, InfoMat (2023), https://doi.org/10.1002/inf2.12418.

[30] H.J. Hwang, J.H. Yang, Y.G. Lee, C. Cho, C.G. Kang, S.C. Kang, W. Park, B.H. Lee, Ferroelectric polymer-gated graphene memory with high speed conductivity modulation, Nanotechnology 24 (2013) 175202, https://doi.org/10.1088/0957-4484/24/17/175202.

[31] S. Maity, C. Kulsi, S. Banerjee, S. Das, K. Chatterjee, Dependence of thermoelectric power and electrical conductivity on structural order of PEDOT-Tos-graphene nanocomposite via charge carrier mobility, Mater. Res. Express 6 (2019) 105095, https://doi.org/10.1088/2053-1591/ab3e7c.

[32] M. Kaddes, M. Zemzemi, Computational study of electronic and thermoelectric properties of ZnO/graphene heterostructures, Int. J. Thermophys. 42 (2021) 100, https://doi.org/10.1007/s10765-021-02854-5.

[33] P. Dollfus, V. Hung Nguyen, J. Saint-Martin, Thermoelectric effects in graphene nanostructures, J. Phys. Condens. Matter 27 (2015) 133204, https://doi.org/10.1088/0953-8984/27/13/133204.

[34] Y. Xu, Z. Li, W. Duan, Thermal and thermoelectric properties of graphene, Small 10 (2014) 2182–2199, https://doi.org/10.1002/smll.201303701.

[35] P. an Zong, J. Liang, P. Zhang, C. Wan, Y. Wang, K. Koumoto, Graphene-based thermoelectrics, ACS Appl. Energy Mater. 3 (2020) 2224–2239, https://doi.org/10.1021/acsaem.9b02187.

[36] A.A. Balandin, S. Ghosh, W. Bao, I. Calizo, D. Teweldebrhan, F. Miao, C.N. Lau, Superior thermal conductivity of single-layer graphene, Nano Lett. 8 (2008) 902–907, https://doi.org/10.1021/nl0731872.

[37] A.H. Castro Neto, F. Guinea, N.M.R. Peres, K.S. Novoselov, A.K. Geim, The electronic properties of graphene, Rev. Mod. Phys. 81 (2009) 109–162, https://doi.org/10.1103/RevModPhys.81.109.

[38] S. Das Sarma, S. Adam, E.H. Hwang, E. Rossi, Electronic transport in two-dimensional graphene, Rev. Mod. Phys. 83 (2011) 407–470, https://doi.org/10.1103/RevModPhys.83.407.

[39] Y. Anno, Y. Imakita, K. Takei, S. Akita, T. Arie, Enhancement of graphene thermoelectric performance through defect engineering, 2D Mater. 4 (2017) 025019, https://doi.org/10.1088/2053-1583/aa57fc.

[40] E. Rahmati, A. Bafekry, M. Faraji, D. Gogva, C.V. Nguyen, M. Ghergherehchi, Thermoelectric properties of doped graphene nanoribbons: density functional theory calculations and electrical transport, RSC Adv. 12 (2022) 6174–6180, https://doi.org/10.1039/D1RA08303A.

[41] S. Ullah, Q. Shi, J. Zhou, X. Yang, H.Q. Ta, M. Hasan, N.M. Ahmad, L. Fu, A. Bachmatiuk, M.H. Rümmeli, Advances and trends in chemically doped graphene, Adv Mater Interfaces 7 (2020) 2000999, https://doi.org/10.1002/admi.202000999.

[42] M. Sharafat Hossain, F. Al-Dirini, F.M. Hossain, E. Skafidas, High performance graphene nano-ribbon thermoelectric devices by incorporation and dimensional tuning of nanopores, Sci. Rep. 5 (2015) 11297, https://doi.org/10.1038/srep11297.

[43] J. Mu, C. Hou, H. Wang, Y. Li, Q. Zhang, Graphene-carbon nanotube papers for energy conversion and storage under sunlight and heat, Carbon N Y 95 (2015) 150–156, https://doi.org/10.1016/j.carbon.2015.08.027.

[44] Y. Guo, J. Mu, C. Hou, H. Wang, Q. Zhang, Y. Li, Flexible and thermostable thermoelectric devices based on large-area and porous all-graphene films, Carbon N Y 107 (2016) 146–153, https://doi.org/10.1016/j.carbon.2016.05.063.

[45] M.S. Hossain, D.H. Huynh, P.D. Nguyen, L. Jiang, T.C. Nguyen, F. Al-Dirini, F. M. Hossain, E. Skafidas, Enhanced thermoelectric performance of graphene nanoribbon-based devices, J. Appl. Phys. 119 (2016), https://doi.org/10.1063/1.4944710.

[46] N.D.K. Tu, J.A. Lim, H. Kim, A mechanistic study on the carrier properties of nitrogen-doped graphene derivatives using thermoelectric effect, Carbon N Y 117 (2017) 447–453, https://doi.org/10.1016/j.carbon.2017.03.009.

[47] D. Geng, S. Yang, Y. Zhang, J. Yang, J. Liu, R. Li, T.K. Sham, X. Sun, S. Ye, S. Knights, Nitrogen doping effects on the structure of graphene, Appl. Surf. Sci. 257 (2011) 9193–9198, https://doi.org/10.1016/j.apsusc.2011.05.131.

[48] H. Xu, L. Ma, Z. Jin, Nitrogen-doped graphene: synthesis, characterizations and energy applications, J. Energy Chem. 27 (2018) 146–160, https://doi.org/10.1016/j.jechem.2017.12.006.

[49] K. Gong, F. Du, Z. Xia, M. Durstock, L. Dai, Nitrogen-doped carbon nanotube arrays with high electrocatalytic activity for oxygen reduction, Science 323 (2009) 760–764, https://doi.org/10.1126/science.1168049, 1979.

[50] S.U. Lee, R.V. Belosludov, H. Mizuseki, Y. Kawazoe, Designing nanogadgetry for nanoelectronic devices with nitrogen-doped capped carbon nanotubes, Small 5 (2009) 1769–1775, https://doi.org/10.1002/smll.200801938.

[51] Y. Zhang, K. Fugane, T. Mori, L. Niu, J. Ye, Wet chemical synthesis of nitrogen-doped graphene towards oxygen reduction electrocatalysts without high-temperature pyrolysis, J. Mater. Chem. 22 (2012) 6575–6580, https://doi.org/10.1039/c2jm00044j.

[52] L. Qu, Y. Liu, J.B. Baek, L. Dai, Nitrogen-doped graphene as efficient metal-free electrocatalyst for oxygen reduction in fuel cells, ACS Nano 4 (2010) 1321–1326, https://doi.org/10.1021/nn901850u.

[53] D. Wei, Y. Liu, Y. Wang, H. Zhang, L. Huang, G. Yu, Synthesis of n-doped graphene by chemical vapor deposition and its electrical properties, Nano Lett. 9 (2009) 1752–1758, https://doi.org/10.1021/nl803279t.

[54] Y.J. Cho, H.S. Kim, H. Im, Y. Myung, G.B. Jung, C.W. Lee, J. Park, M.H. Park, J. Cho, H.S. Kang, Nitrogen-doped graphitic layers deposited on silicon nanowires for efficient lithium-ion battery anodes, J. Phys. Chem. C 115 (2011) 9451–9457, https://doi.org/10.1021/jp201485j.

[55] Y. Xue, B. Wu, L. Jiang, Y. Guo, L. Huang, J. Chen, J. Tan, D. Geng, B. Luo, W. Hu, G. Yu, Y. Liu, Low temperature growth of highly nitrogen-doped single crystal graphene arrays by chemical vapor deposition, J. Am. Chem. Soc. 134 (2012) 11060–11063, https://doi.org/10.1021/ja302483t.

[56] Z. Jin, J. Yao, C. Kittrell, J.M. Tour, Large-scale growth and characterizations of nitrogen-doped monolayer graphene sheets, ACS Nano 5 (2011) 4112–4117, https://doi.org/10.1021/nn200766e.

[57] H. Gao, L. Song, W. Guo, L. Huang, D. Yang, F. Wang, Y. Zuo, X. Fan, Z. Liu, W. Gao, R. Vajtai, K. Hackenberg, P.M. Ajayan, A simple method to synthesize continuous large area nitrogen-doped graphene, Carbon N Y 50 (2012) 4476–4482, https://doi.org/10.1016/j.carbon.2012.05.026.

[58] J. Bai, Q. Zhu, Z. Lv, H. Dong, J. Yu, L. Dong, Nitrogen-doped graphene as catalysts and catalyst supports for oxygen reduction in both acidic and alkaline solutions, Int. J. Hydrogen Energy 38 (2013) 1413–1418, https://doi.org/10.1016/j.ijhydene.2012.11.039.

[59] D. Deng, X. Pan, L. Yu, Y. Cui, Y. Jiang, J. Qi, W.X. Li, Q. Fu, X. Ma, Q. Xue, G. Sun, X. Bao, Toward N-doped graphene via solvothermal synthesis, Chem. Mater. 23 (2011) 1188–1193, https://doi.org/10.1021/cm102666r.

[60] Z. Jin, Z. Sun, L.J. Simpson, K.J. O'Neill, P.A. Parilla, Y. Li, N.P. Stadie, C.C. Ahn, C. Kittrell, J.M. Tour, Solution-phase synthesis of heteroatom-substituted carbon scaffolds for hydrogen storage, J. Am. Chem. Soc. 132 (2010) 15246–15251, https://doi.org/10.1021/ja105428d.

[61] B. Xiong, Y. Zhou, R. O'Hayre, Z. Shao, Facile single-step ammonia heat-treatment and quenching process for the synthesis of improved Pt/N-graphene catalysts, Appl. Surf. Sci. 266 (2013) 433–439, https://doi.org/10.1016/j.apsusc.2012.12.053.

[62] B. Guo, Q. Liu, E. Chen, H. Zhu, L. Fang, J.R. Gong, Controllable N-doping of graphene, Nano Lett. 10 (2010) 4975–4980, https://doi.org/10.1021/nl103079j.

[63] B. Jiang, C. Tian, L. Wang, L. Sun, C. Chen, X. Nong, Y. Qiao, H. Fu, Highly concentrated, stable nitrogen-doped graphene for supercapacitors: simultaneous doping and reduction, Appl. Surf. Sci. 258 (2012) 3438–3443, https://doi.org/10.1016/j.apsusc.2011.11.091.

[64] H. Peng, Z. Mo, S. Liao, H. Liang, L. Yang, F. Luo, H. Song, Y. Zhong, B. Zhang, High performance Fe- and N- Doped carbon catalyst with graphene structure for oxygen reduction, Sci. Rep. 3 (2013), https://doi.org/10.1038/srep01765.

[65] Z. Lin, G.H. Waller, Y. Liu, M. Liu, C. ping Wong, 3D Nitrogen-doped graphene prepared by pyrolysis of graphene oxide with polypyrrole for electrocatalysis of oxygen reduction reaction, Nano Energy 2 (2013) 241–248, https://doi.org/10.1016/j.nanoen.2012.09.002.

[66] Y. Wang, Y. Shao, D.W. Matson, J. Li, Y. Lin, Nitrogen-doped graphene and its application in electrochemical biosensing, ACS Nano 4 (2010) 1790–1798, https://doi.org/10.1021/nn100315s.

[67] H.M. Jeong, J.W. Lee, W.H. Shin, Y.J. Choi, H.J. Shin, J.K. Kang, J.W. Choi, Nitrogen-doped graphene for high-performance ultracapacitors and the importance of nitrogen-doped sites at basal planes, Nano Lett. 11 (2011) 2472–2477, https://doi.org/10.1021/nl2009058.

[68] N. Li, Z. Wang, K. Zhao, Z. Shi, Z. Gu, S. Xu, Large scale synthesis of N-doped multi-layered graphene sheets by simple arc-discharge method, Carbon N Y 48 (2010) 255–259, https://doi.org/10.1016/j.carbon.2009.09.013.

[69] J.O. Hwang, J.S. Park, D.S. Choi, J.Y. Kim, S.H. Lee, K.E. Lee, Y.H. Kim, M. H. Song, S. Yoo, S.O. Kim, Workfunction-tunable, N-doped reduced graphene transparent electrodes for high-performance polymer light-emitting diodes, ACS Nano 6 (2012) 159–167, https://doi.org/10.1021/nn203176u.

[70] S. Seo, Y. Yoon, J. Lee, Y. Park, H. Lee, Nitrogen-doped partially reduced graphene oxide rewritable nonvolatile memory, ACS Nano 7 (2013) 3607–3615, https://doi.org/10.1021/nn400588u.

[71] H. Fan, Y. Li, D. Wu, H. Ma, K. Mao, D. Fan, B. Du, H. Li, Q. Wei, Electrochemical bisphenol A sensor based on N-doped graphene sheets, Anal. Chim. Acta 711 (2012) 24–28, https://doi.org/10.1016/j.aca.2011.10.051.

[72] E.K. Goharshadi, S.J. Mahdizadeh, Thermal conductivity and heat transport properties of nitrogen-doped graphene, J. Mol. Graph. Model. 62 (2015) 74–80, https://doi.org/10.1016/j.jmgm.2015.09.008.

[73] W. Yu, L. Wang, Y. Qi, L. Chen, L. Wang, H. Xie, The influence of nitrogen doping on thermal conductivity of carbon nanotubes, Thermochim. Acta 617 (2015) 163–168, https://doi.org/10.1016/j.tca.2015.08.034.

[74] K.T. Chan, J.B. Neaton, M.L. Cohen, First-principles study of metal adatom adsorption on graphene, Phys. Rev. B 77 (2008) 235430, https://doi.org/10.1103/PhysRevB.77.235430.

[75] K. Nakada, A. Ishii, Migration of adatom adsorption on graphene using DFT calculation, Solid State Commun. 151 (2011) 13–16, https://doi.org/10.1016/j.ssc.2010.10.036.

[76] L. Semidey-Flecha, D. Teng, B.F. Habenicht, D.S. Sholl, Y. Xu, Adsorption and diffusion of the Rh and Au adatom on graphene moiré/Ru(0001), J. Chem. Phys. 138 (2013) 184710, https://doi.org/10.1063/1.4803893.

[77] W. Hu, L. Lin, C. Yang, J. Yang, Electronic structure and aromaticity of large-scale hexagonal graphene nanoflakes, J. Chem. Phys. 141 (2014) 214704, https://doi.org/10.1063/1.4902806.

[78] R.G. Parr, W. Yang, Density functional approach to the frontier-electron theory of chemical reactivity, J. Am. Chem. Soc. 106 (1984) 4049–4050, https://doi.org/10.1021/ja00326a036.

[79] W. Kohn, L.J. Sham, Self-consistent equations including exchange and correlation effects, Phys. Rev. 140 (1965) A1133–A1138, https://doi.org/10.1103/PhysRev.140.A1133.

[80] P. Hohenberg, W. Kohn, Inhomogeneous electron gas, Phys. Rev. 136 (1964) 3B, https://doi.org/10.1103/PhysRev.136.B864.

[81] T. Ozaki, H. Kino, J. Yu, M.J. Han, M. Ohfuchi, F. Ishii, K. Sawada, Y. Kubota, Y. P. Mizuta, H. Kotaka, N. Yamaguchi, H. Sawahata, T.B. Prayitno, T. Ohwaki, T.V. T. Duy, M. Miyata, G. Jiang, P.H. Chang, A. Terasawa, Y. Gohda, H. Weng, Y. Shiihara, M. Toyoda, Y. Okuno, R. Perez, P.P. Bell, M. Ellner, Y. Xiao, A.M. Ito, M. Otani, M. Kawamura, K. Yoshimi, C.C. Lee, Y.T. Lee, M. Fukuda, S. Ryee, K. Terakura, User's Manual of OpenMX Ver. 3.9, 2020 (Tokyo).

[82] T. Ozaki, Variationally optimized atomic orbitals for large-scale electronic structures, Phys. Rev. B 67 (2003) 155108, https://doi.org/10.1103/PhysRevB.67.155108.

[83] T. Ozaki, H. Kino, Numerical atomic basis orbitals from H to Kr, Phys. Rev. B 69 (2004) 195113, https://doi.org/10.1103/PhysRevB.69.195113.

[84] N. Troullier, J.L. Martins, Efficient pseudopotentials for plane-wave calculations, Phys. Rev. B 43 (1991) 1993, https://doi.org/10.1103/PhysRevB.43.1993.–2006.

[85] K. Lejaeghere, G. Bihlmayer, T. Björkman, P. Blaha, S. Blügel, V. Blum, D. Caliste, I.E. Castelli, S.J. Clark, A. Dal Corso, S. de Gironcoli, T. Deutsch, J.K. Dewhurst, I. Di Marco, C. Draxl, M. Dułak, O. Eriksson, J.A. Flores-Livas, K.F. Garrity, L. Genovese, P. Giannozzi, M. Giantomassi, S. Goedecker, X. Gonze, O. Grånäs, E. K.U. Gross, A. Gulans, F. Gygi, D.R. Hamann, P.J. Hasnip, N.A.W. Holzwarth, D. Iuşan, D.B. Jochym, F. Jollet, D. Jones, G. Kresse, K. Koepernik, E. Küçükbenli, Y.O. Kvashnin, I.L.M. Locht, S. Lubeck, M. Marsman, N. Marzari, U. Nitzsche, L. Nordström, T. Ozaki, L. Paulatto, C.J. Pickard, W. Poelmans, M.I.J. Probert, K. Refson, M. Richter, G.-M. Rignanese, S. Saha, M. Scheffler, M. Schlipf, K. Schwarz, S. Sharma, F. Tavazza, P. Thunström, A. Tkatchenko, M. Torrent, D. Vanderbilt, M.J. van Setten, V. Van Speybroeck, J.M. Wills, J.R. Yates, G.-X. Zhang, S. Cottenier, Reproducibility in density functional theory calculations of solids, Science (2016) 351, https://doi.org/10.1126/science.aad3000, 1979.

[86] J.P. Perdew, K. Burke, M. Ernzerhof, Generalized gradient approximation made simple, Phys. Rev. Lett. 77 (1996) 3865–3868, https://doi.org/10.1103/PhysRevLett.77.3865.

[87] G.K.H. Madsen, D.J. Singh, BoltzTraP. A code for calculating band-structure dependent quantities, Comput. Phys. Commun. 175 (2006) 67–71, https://doi.org/10.1016/j.cpc.2006.03.007.

[88] M. Miyata, T. Ozaki, T. Takeuchi, S. Nishino, M. Inukai, M. Koyano, High-throughput screening of sulfide thermoelectric materials using electron transport calculations with OpenMX and BoltzTraP, J. Electron. Mater. 47 (2018) 3254–3259, https://doi.org/10.1007/s11664-017-6020-9.

[89] X. Lin, J. Ni, Much stronger binding of metal adatoms to silicene than to graphene: a first-principles study, Phys. Rev. B 86 (2012) 075440, https://doi.org/10.1103/PhysRevB.86.075440.

[90] P. Rani, V.K. Jindal, Designing band gap of graphene by B and N dopant atoms, RSC Adv. 3 (2013) 802–812, https://doi.org/10.1039/C2RA22664B.

[91] J. Padmanabhan, R. Parthasarathi, V. Subramanian, P.K. Chattaraj, Electrophilicity-based charge transfer descriptor, J. Phys. Chem. A 111 (2007) 1358–1361, https://doi.org/10.1021/jp0649549.

[92] S. Nath, Thermoelectric and optical properties of 2D hexagonal Dirac material Be_3X_2 (X = C, Si, Ge, Sn): a density functional theory study, J. Appl. Phys. 130 (2021), https://doi.org/10.1063/5.0059942.

[93] F. Kong, Y. Hu, H. Hou, Y. Liu, B. Wang, L. Wang, Thermoelectric and thermodynamic properties of half-Heulser alloy YPdSb from first principles calculations, J. Solid State Chem. 196 (2012) 511–517, https://doi.org/10.1016/j.jssc.2012.07.010.

[94] P. Lubis, N. Amalia, S.A. Wella, S. Sholihun, Thermoelectric properties of monolayer and bilayer buckled XTe (X = Ge, Sn, and Pb), Adv. Nat. Sci. Nanosci. Nanotechnol. 13 (2022) 025008, https://doi.org/10.1088/2043-6262/ac7322.

[95] U.S. Shenoy, D.K. Bhat, Vanadium-doped $BaTiO_3$ as high performance thermoelectric material: role of electronic structure engineering, Mater. Today Chem. 18 (2020) 100384, https://doi.org/10.1016/j.mtchem.2020.100384.

[96] D.K. Bhat, S. Shenoy U, High thermoelectric performance of Co-doped tin telluride due to synergistic effect of magnesium and indium, J. Phys. Chem. C 121 (2017) 7123–7130, https://doi.org/10.1021/acs.jpcc.7b00870.

[97] U.S. Shenoy, D.K. Bhat, Bi and Zn co-doped SnTe thermoelectrics: interplay of resonance levels and heavy hole band dominance leading to enhanced

performance and a record high room temperature *ZT*, J Mater Chem C Mater 8 (2020) 2036–2042, https://doi.org/10.1039/C9TC06490G.
[98] U.S. Shenoy, D.K. Bhat, Electronic structure engineering of tin telluride through co-doping of bismuth and indium for high performance thermoelectrics: a synergistic effect leading to a record high room temperature *ZT* in tin telluride, J Mater Chem C Mater 7 (2019) 4817–4821, https://doi.org/10.1039/C9TC01184F.
[99] N.I. Verbitskiy, A.V. Fedorov, G. Profeta, A. Stroppa, L. Petaccia, B. Senkovskiy, A. Nefedov, C. Wöll, D.Yu Usachov, D.V. Vyalikh, L.V. Yashina, A.A. Eliseev, T. Pichler, A. Grüneis, Atomically precise semiconductor—graphene and hBN interfaces by Ge intercalation, Sci. Rep. 5 (2015) 17700, https://doi.org/10.1038/srep17700.
[100] J.L. McChesney, A. Bostwick, T. Ohta, T. Seyller, K. Horn, J. González, E. Rotenberg, Extended van Hove singularity and superconducting instability in doped graphene, Phys. Rev. Lett. 104 (2010) 136803, https://doi.org/10.1103/PhysRevLett.104.136803.
[101] J. Sforzini, P. Hapala, M. Franke, G. van Straaten, A. Stöhr, S. Link, S. Soubatch, P. Jelínek, T.-L. Lee, U. Starke, M. Švec, F.C. Bocquet, F.S. Tautz, Structural and electronic properties of nitrogen-doped graphene, Phys. Rev. Lett. 116 (2016) 126805, https://doi.org/10.1103/PhysRevLett.116.126805.
[102] D.Yu Usachov, A.V. Fedorov, O.Yu Vilkov, B.V. Senkovskiy, V.K. Adamchuk, B. V. Andryushechkin, D.V. Vyalikh, Synthesis and electronic structure of nitrogen-doped graphene, Phys. Solid State 55 (2013) 1325–1332, https://doi.org/10.1134/S1063783413060310.
[103] L. Daukiya, M.N. Nair, S. Hajjar-Garreau, F. Vonau, D. Aubel, J.L. Bubendorff, M. Cranney, E. Denys, A. Florentin, G. Reiter, L. Simon, Highly n-doped graphene generated through intercalated terbium atoms, Phys. Rev. B 97 (2018) 035309, https://doi.org/10.1103/PhysRevB.97.035309.
[104] M. Scardamaglia, C. Struzzi, S. Osella, N. Reckinger, J.-F. Colomer, L. Petaccia, R. Snyders, D. Beljonne, C. Bittencourt, Tuning nitrogen species to control the charge carrier concentration in highly doped graphene, 2D Mater. 3 (2016) 011001, https://doi.org/10.1088/2053-1583/3/1/011001.
[105] N. Poudel, S.J. Liang, D. Choi, B. Hou, L. Shen, H. Shi, L.K. Ang, L. Shi, S. Cronin, Cross-plane thermoelectric and thermionic transport across Au/h-BN/Graphene heterostructures, Sci. Rep. 7 (2017), https://doi.org/10.1038/s41598-017-12704-w.
[106] Y. Anno, Y. Imakita, K. Takei, S. Akita, T. Arie, Enhancement of graphene thermoelectric performance through defect engineering, 2D Mater. 4 (2017), https://doi.org/10.1088/2053-1583/aa57fc.
[107] L. Wang, Q. Yao, H. Bi, F. Huang, Q. Wang, L. Chen, Large thermoelectric power factor in polyaniline/graphene nanocomposite films prepared by solution-assistant dispersing method, J Mater Chem A Mater 2 (2014) 11107–11113, https://doi.org/10.1039/c4ta01541j.
[108] Z. Jing, H. Wang, X. Feng, B. Xiao, Y. Ding, K. Wu, Y. Cheng, Superior thermoelectric performance of ordered double transition metal MXenes: $Cr_2TiC_2T_2$ (T = -OH or -F), J. Phys. Chem. Lett. 10 (2019) 5721–5728, https://doi.org/10.1021/acs.jpclett.9b01827.
[109] S. Karmakar, T. Saha-Dasgupta, First-principles prediction of enhanced thermoelectric properties of double transition metal MXenes: Ti3-xMox C2T2; (x=0.5,1,1.5,2,2.5,T=-OH/- O/- F), Phys. Rev. Mater. 4 (2020), https://doi.org/10.1103/PhysRevMaterials.4.124007.
[110] X. Lu, Q. Zhang, J. Liao, H. Chen, Y. Fan, J. Xing, S. Gu, J. Huang, J. Ma, J. Wang, L. Wang, W. Jiang, High-efficiency thermoelectric power generation enabled by homogeneous Incorporation of MXene in (Bi,Sb)2Te3 Matrix, Adv. Energy Mater. 10 (2020), https://doi.org/10.1002/aenm.201902986.
[111] H. Sadeghi, S. Sangtarash, C.J. Lambert, Cross-plane enhanced thermoelectricity and phonon suppression in graphene/MoS2 van der Waals heterostructures, 2D Mater. 4 (2017), https://doi.org/10.1088/2053-1583/4/1/015012.
[112] X. Wang, M. Zebarjadi, K. Esfarjani, First principles calculations of solid-state thermionic transport in layered van der Waals heterostructures, Nanoscale 8 (2016) 14695–14704, https://doi.org/10.1039/c6nr02436j.
[113] X. Wang, M. Zebarjadi, K. Esfarjani, High-performance solid-state thermionic energy conversion based on 2D van der Waals heterostructures: a first-principles study, Sci. Rep. 8 (2018), https://doi.org/10.1038/s41598-018-27430-0.
[114] S.N. Alam, N. Sharma, L. Kumar, Synthesis of graphene oxide (GO) by modified Hummers method and its thermal reduction to Obtain reduced graphene oxide (rGO), Graphene 6 (2017) 1–18, https://doi.org/10.4236/graphene.2017.61001.
[115] N. Kumar, P.K. Sachdeva, R. Gupta, C. Bera, Theoretical design of highly efficient 2D thermoelectric device based on janus MoSSe and graphene heterostructure, ACS Appl. Energy Mater. 5 (2022) 9581–9586, https://doi.org/10.1021/acsaem.2c01204.
[116] Y. Zheng, J. Gao, C. Han, W. Chen, Ohmic contact engineering for two-dimensional materials, Cell Rep Phys Sci 2 (2021), https://doi.org/10.1016/j.xcrp.2020.100298.
[117] Y.S. Ang, L. Cao, L.K. Ang, Physics of electron emission and injection in two-dimensional materials: theory and simulation, InfoMat 3 (2021) 502–535, https://doi.org/10.1002/inf2.12168.